Available online at www.sciencedirect.com
ScienceDirect
Journal of Sound and Vibration 319 (2009) 426–444
JOURNAL OF SOUND AND VIBRATION
www.elsevier.com/locate/jsvi

Prediction of averaged energy for moderately damped systems with strong coupling

S. Wang, R.J. Bernhard*

Ray W. Herrick Laboratories, School of Mechanical Engineering, Purdue University, West Lafayette, IN 47907-1077, USA

Received 7 March 2007; received in revised form 3 February 2008; accepted 21 April 2008
Handling Editor: S. Bolton

Abstract

In this paper, the prediction of averaged energy of damped structural-acoustic systems is investigated. A simplified energy finite element method, referred to as EFEM^0, is developed based on the energy flow analysis (EFA) equations and implemented using the finite volume method. The resulting formulations can be incorporated into statistical energy analysis (SEA) software and extends SEA application to moderately damped systems with strong coupling. The formulations are verified against analytical solutions for a single beam and coupled beams with both strong and weak coupling. A hybrid technique consisting of the EFEM^0 approximation superimposed on a direct field is used to model moderately damped plates. For lightly damped systems, both methods produce acceptable results. For moderately damped two-dimensional systems, the EFEM^0 method augmented with the direct field component produces significantly improved results.

1. Introduction

The prediction of averaged energy of structural-acoustic system is often sufficient for the purpose of design, particularly for broadband excitation or when frequency-averaged results are desired. This type of prediction is common, particularly using statistical energy analysis (SEA). SEA theories were developed assuming light damping and weak coupling. For such systems, the subsystems are reverberant and the energy density within the subsystems can be assumed to be uniform. The coupling of subsystems will not depend on the relative location or orientation of the subsystems, only that they are connected.

On the other hand, the energy response of systems with heavy damping tends to be dominated by response directly from the source. Since the energy is dissipated throughout the subsystems, the energy scattered at the boundaries is minimal and does not create a significant "reverberant" or diffuse field. For heavily damped systems, direct field theories will model response well except near the boundaries.

For systems where damping is moderate, the energy density within the system is higher near the source due to the direct field but becomes more uniform away from the source as reflections from the boundaries become more significant. In such cases the energy within subsystems is spatially varying. In addition, the energy transmitted through the joint between two subsystems is dependent on the energy incident on the joint, which

*Corresponding author. Fax: +1 765 494 0787.
E-mail addresses: rbernhar@nd.edu, bernhard@ecn.purdue.edu (R.J. Bernhard).

0022-460X/$ - see front matter © 2008 Published by Elsevier Ltd.
doi:10.1016/j.jsv.2008.04.048

is determined by the relative location of the joint to the source(s). In a built-up system where energy is transmitted through multiple moderately damped subsystems, the effect of spatial location can accumulate to significantly affect the predicted energy in the remote subsystems. Average energy models that make many of the same assumptions as SEA but account for the effects of moderate damping are available and are sometimes referred to as energy flow analysis (EFA). In addition to modeling moderate damping, these theories are also capable of modeling the behavior of strong coupling. The methods and predictions based on the different theories will be compared for simple systems with different levels of damping.

2. Energy flow analysis theory

To obtain an accurate and simple mathematical model representing the energy propagation in structural-acoustic systems, significant efforts have been made to develop equations that govern the energy flow in continuous structures. Belov and Rybak first derived the transport equations utilizing the Green's function for infinite vibrating plates [1], and formulated the conduction equations for the energy flow in ribbed plates [2]. Nefske and Sung [3] developed the equation that governs the energy flow in homogeneous finite beams and solved the equation in terms of energy variables. Wohlever and Bernhard [4] derived the energy governing equations using a method that is consistent with classical mechanics, and obtained a second-order differential equation which governs the smoothed energy distribution in rods and beams. The coupling of subsystems in terms of energy density was developed by Cho [5]. Using these governing differential equations and coupling relations to solve the energy variables analytically is referred to here as EFA. By this approach, energy conduction in structural-acoustic systems is simple to predict and can be implemented using numerical methods with relatively few degrees of freedom. The technique predicts the spatial distribution of the energetics of built-up structures if the energy density is spatially varying.

SEA was initiated by Lyon and Maidanik [6]. The basic premise of SEA is to represent the state of vibration by stored, dissipated, and transferred energies. For SEA approximations, the lumped physical dynamical characteristics of the subsystems are used to describe the system. This feature makes SEA a simple, straightforward method with inexpensive computational cost. SEA has been extended from the original theories and has been successfully used for numerous cases. However, application is limited by the underlying assumptions of SEA theory. For example, SEA assumes energy is evenly distributed within a subsystem. This assumption limits application of SEA to lightly damped systems where the energy incident on a joint is not dependent on the location of the joint relative to the source(s). Guyader et al. [7] have shown that SEA overestimates the energy transmission between two coupled plates in an L-shape. SEA application is also limited by the assumption of light coupling which prohibits dividing a natural subsystem, such as an acoustical enclosure, into multiple elements.

In the following subsections, the principles of EFA will be summarized and a simple numerical implementation of the EFA equations will be developed and compared to SEA. This numerical formulation, referred to as EFEM^0 (the superscript "0" denoting that a zero-order interpolation or the finite volume method is applied [8]), is a moderate extension of SEA and is possible to implement using SEA software. Predictions using the various methods will be compared for point excited, one-dimensional (1-D) and damped two-dimensional (2-D)systems where concern has been expressed about EFA-based methods [9].

2.1. The EFA system model

For steady-state vibrational energy propagation within a control volume V, the principle of conservation of energy requires that the total power Π_{in} entering the control volume must be balanced by the summation of the power dissipated in the volume, Π_{diss}, and the energy flow through the boundary S:

$$\Pi_{\text{diss}} += \Pi_{\text{in}}, \tag{1}$$

where $\vec{I}$ is the intensity of the field. For a general case, assuming the intensity function has continuous first partial derivatives, the divergence theorem can be applied such that

$$\int_S \vec{I} \cdot \vec{n}\, \mathrm{d}A = \int_V \nabla \cdot \vec{I}\, \mathrm{d}V. \tag{2}$$

Writing each term in Eq. (1) in the format of volume integrals

$$\int_V \pi_{\text{diss}}\,\mathrm{d}V + \int_V \nabla\cdot\overrightarrow{I}\,\mathrm{d}V = \int_V \pi_{\text{in}}\,\mathrm{d}V, \tag{3}$$

the energy balance equation is obtained for steady-state vibrational energy propagation such that

$$\nabla\cdot\overrightarrow{I} + \pi_{\text{diss}} = \pi_{\text{in}}, \tag{4}$$

where π_{in} is the input power density (power input per unit volume), π_{diss} is the dissipated power density (power dissipated per unit volume). For EFA implementations a simple loss factor model of damping is used for power dissipation

$$\pi_{\text{diss}} = \eta\omega e, \tag{5}$$

where η is the damping loss factor, ω is the angular frequency, and e is the time-averaged and locally space-averaged energy density.

As derived by Bouthier and Bernhard [10], the relationship between energy density and intensity for a point-excited infinite plate is

$$\nabla\cdot\vec{I} = \frac{1}{r}\frac{\mathrm{d}}{\mathrm{d}r}(rc_g e). \tag{6}$$

Using Eqs. (4)–(6), the governing differential equation for energy density distribution in the far field of a infinite point-excited plate is [10]

$$\frac{1}{r}\frac{\mathrm{d}}{\mathrm{d}r}(rc_g e_d) + \eta\omega e = \pi_{\text{in}}. \tag{7}$$

The solution for the direct-field energy density due to a point source in a two-dimensional system is

$$e_d = \frac{\Pi_{\text{in}}}{2\pi hrc_g}\exp(-\eta\omega r/c_g) \tag{8}$$

and the radial intensity is

$$I_{\text{rad}} = c_g e_d(R) = \frac{\Pi_{\text{in}}}{2\pi hr}\exp(-\eta\omega r/c_g). \tag{9}$$

A similar equation can be derived for three-dimensional (3-D) homogeneous systems using Bouthier and Bernhard [10] but will not be derived or used in this paper.

For certain cases, such as in a reverberant field, where the response can be assumed to be the superposition of moderately damped plane waves, Bouthier and Bernhard [10] showed that the smoothed intensity $\overrightarrow{I}$ is related to the energy density by

$$\overrightarrow{I} = -\left(\frac{c_g^2}{\eta\omega}\right)\nabla e, \tag{10}$$

where e is the time-averaged and locally space-averaged energy density, ∇e is the gradient of the smoothed energy density, and c_g is the group speed. Using Eqs. (4), (5) and (10), the general form of the differential equation governing the energy density in an isotropic, homogenous system can be written as

$$\left(\frac{c_g^2}{\omega\eta}\right)\nabla^2 e - \omega\eta e + \pi_{\text{in}} = 0. \tag{11}$$

2.2. EFA joint model

For structural problems, discontinuity of physical properties causes the energy density to be discontinuous at joints. However, as described by Cho [5], using smoothing approximations that are consistent with EFA

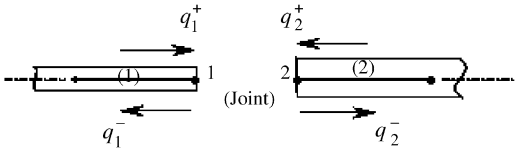

Fig. 1. Two co-linear beam elements coupled with a joint.

equations, a relationship between energy flow and energy density at the joint can be found. To illustrate the derivation of this relationship for a simple example of two coupled systems, consider the case of two coupled collinear beams as shown in Fig. 1. The energy density and energy flow at joints with discontinuities can be expressed in terms of components associated with positive (+) and negative (−) traveling waves:

$$e_i = e_i^+ + e_i^- \tag{12}$$

and

$$q_i = q_i^+ - q_i^- = c_{gi}e_i^+A_i - c_{gi}e_i^-A_i \quad (i = 1, 2). \tag{13}$$

where A is the cross-sectional area, and c_g is the group speed. At the joint position, e_i ($i = 1, 2$) are the nodal values of energy density on either side of the joint and q_i ($i = 1, 2$) are the net energy flow through the joint out of beam i.

For the coupled collinear systems as shown in Fig. 1, the net energy flow away from the joint in each beam can be expressed as

$$q_2^- = \tau_{12}q_1^+ + r_{22}q_2^+, \tag{14}$$

$$q_1^- = \tau_{21}q_2^+ + r_{11}q_1^+, \tag{15}$$

where τ_{ij} is the power transmission coefficient from beam i to beam j ($i, j = 1, 2$), and r_{ii} is the power reflection coefficient in beam i.

Substituting Eq. (12) and (13) into Eqs. (14) and (15) gives

$$c_{g2}e_2^-A_2 = \tau_{12}c_{g1}e_1^+A_1 + r_{22}c_{g2}e_2^+A_2, \tag{16}$$

$$c_{g1}e_1^-A_1 = \tau_{21}c_{g2}e_2^+A_2 + r_{11}c_{g1}e_1^+A_1. \tag{17}$$

The relationship between net energy flow and energy density are obtained by solving Eqs. (12)–(17). Substituting the values of $e_i^{\pm}$ into Eq. (13) yields the expression of energy flow through the joint from beam 1, which is also the energy flow from beam 1 to 2:

$$q_{1\to 2} = q_1 = \frac{1}{r_{11} + r_{22}}[\tau_{12}c_{g1}A_1 \quad -\tau_{21}c_{g2}A_2]\begin{Bmatrix} e_1 \\ e_2 \end{Bmatrix}. \tag{18}$$

The energy flow from beam 2 to beam 1 is $q_{2\to 1} = q_2 = -q_1$. This same type of joint relationship can be developed in terms of reflection and transmission coefficients for multiple connected joints and distributed joints [11].

The derivation of q_1 and q_2 does not require the joint to be conservative. Thus, it is possible to model a dissipative joint using Eqs. (16) and (17) and EFA methods. For conservative coupling for rods and beams, $\tau_{12} = \tau_{21}$, $r_{11} = r_{22}$ and $\tau + r = 1$. In this paper, the joints are assumed to be conservative. For conservative coupling, the relationship between the energy and energy flow at a joint from Eq. (18) can be reduced to

$$\begin{Bmatrix} q_1 \\ q_2 \end{Bmatrix} = \frac{1}{2 - \tau_{12} - \tau_{21}}\begin{bmatrix} \tau_{12}c_{g1}A_1 & -\tau_{21}c_{g2}A_2 \\ -\tau_{12}c_{g1}A_1 & \tau_{21}c_{g2}A_2 \end{bmatrix}\begin{Bmatrix} e_1 \\ e_2 \end{Bmatrix}. \tag{19}$$

3. Simplified energy finite element method (EFEM^0) model

3.1. EFEM^0 model

In this section, an EFEM^0 formulation will be derived using the finite volume method. The result of the formulation will be a matrix equation much like the SEA matrix equation. The illustration will be developed for a 1-D form of Eq. (11). However, the method can be applied similarly for 2-D and 3-D problems.

The 1-D form of the EFA Eq. (11) can be written as

$$\frac{\mathrm{d}}{\mathrm{d}x}\left(\frac{c_g^2}{\eta\omega}\frac{\mathrm{d}e}{\mathrm{d}x}\right)-\eta\omega e+\pi_{\mathrm{in}}=0. \tag{20}$$

For the finite volume method [12], the problem domain is discretized into a number of control volumes and the center of each control volume is treated as a node. For convenience, we use a capital letter (P, W, or E) to represent both a volume and its center (node), as shown in Fig. 2. The lower case letters "w" and "e" denote the "west" and "east" boundaries of volume (or element) P. The spacing between the nodes is Δx_{WP} and Δx_{PE}. The length of element I (I is any of P, W or E) is identified by L_I.

Integration of the 1-D EFA governing equation over the control volume P yields

$$\begin{aligned}&\int_V \frac{\mathrm{d}}{\mathrm{d}x}\left(\frac{c_g^2}{\eta\omega}\frac{\mathrm{d}e}{\mathrm{d}x}\right)\mathrm{d}V-\int_V(\eta\omega e)\,\mathrm{d}V+\int_V \pi_{\mathrm{in}}\,\mathrm{d}V\\&\quad=\left(\frac{c_g^2A}{\eta\omega}\right)\left.\frac{\mathrm{d}e}{\mathrm{d}x}\right|_e-\left(\frac{c_g^2A}{\eta\omega}\right)\left.\frac{\mathrm{d}e}{\mathrm{d}x}\right|_w-\eta\omega eV+\pi_{\mathrm{in}}V=0,\end{aligned} \tag{21}$$

where $\mathrm{d}V=A\,\mathrm{d}x$ and A is the cross-sectional area of the 1-D system. The volume of P is $V=AL_P$. Eq. (21) is an energy balance equation, which states that the sum of the energy leaving the control volume and the energy dissipated in the domain per unit time is equal to the power input.

The energy flow terms in Eq. (21) can be rewritten as

$$\left(\frac{c_g^2A}{\eta\omega}\right)\left.\frac{\mathrm{d}e}{\mathrm{d}x}\right|_e=\left(\frac{c_g^2A}{\eta\omega}\right)\frac{e_E-e_P}{\Delta x_{PE}},\quad \left(\frac{c_g^2A}{\eta\omega}\right)\left.\frac{\mathrm{d}e}{\mathrm{d}x}\right|_w=\left(\frac{c_g^2A}{\eta\omega}\right)\frac{e_P-e_W}{\Delta x_{WP}}. \tag{22}$$

Substitution of Eq. (22) into Eq. (21) yields

$$\left(\frac{c_g^2A}{\eta\omega}\right)\frac{e_E-e_P}{\Delta x_{PE}}-\left(\frac{c_g^2A}{\eta\omega}\right)\frac{e_P-e_W}{\Delta x_{WP}}-\omega\eta e_PAL_P+\pi_{in}AL_P=0, \tag{23}$$

which can be rearranged as

$$\left(\eta\omega AL_P+\frac{c_g^2A}{\eta\omega\Delta x_{PE}}+\frac{c_g^2A}{\eta\omega\Delta x_{WP}}\right)e_P-\frac{c_g^2A}{\eta\omega\Delta x_{WP}}e_W-\frac{c_g^2A}{\eta\omega\Delta x_{PE}}e_E=\pi_{\mathrm{in}}AL_P. \tag{24}$$

An equation of this form can be developed for each nodal point. The resulting system of linear algebraic equations can be solved to obtain the energy density values at each node. Thus, an approximate spatial distribution of energy density can be obtained for continuous systems. As demonstrated here, one of the major

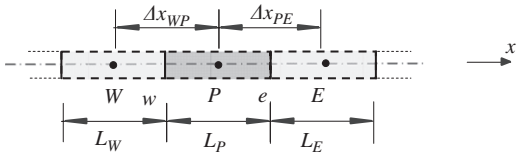

Fig. 2. One-dimensional finite volume grids.

advantages of the finite volume method is that the numerical algorithm is closely related to the underlying physical conservation principle. This feature makes the method easy to apply and to adapt to novel problems.

3.2. Coupling loss factors for strong coupling

To illustrate the relationship of the EFEM^0 to SEA, the energy flow terms in Eq. (23) can also be restated in terms of "coupling" coefficients (η_e^c) and energy conservation. Eq. (23) can be rewritten as

$$\omega[(\eta_{ePE}^c E_P - \eta_{eEP}^c E_E) + (\eta_{ePW}^c E_P - \eta_{eWP}^c E_W)] + \omega\eta E_P = \Pi_{P,\text{in}}, \tag{25}$$

where $E_I = AL_I e_I$, and

$$\eta_{eIJ}^c = \frac{c_g^2}{\eta\omega}\frac{A}{\Delta x_{IJ}}\frac{1}{\omega V_I} = \frac{2c_g^2}{\eta\omega^2 L_I(L_I + L_J)}, \tag{26}$$

where I and J denote the central node numbers of adjacent control volumes (such as E, W, P) and the finite difference approximation $\Delta x_{IJ} = (L_I + L_J)/2$ is used. Eq. (25) is similar to an SEA equation, which has the general form

$$\sum_{j=1,\neq i}^{m} \omega(\eta_{ij}E_i - \eta_{ji}E_j) + \omega\eta_i E_i = \Pi_{i,\text{in}}. \tag{27}$$

For a coupled three-element beam model as shown in Fig. 3, there are two types of couplings: one for the continuous system represented by the connection of elements 1 and 2; the other for the discontinuous system (joint) between elements 2 and 3. According to the coupling relations for the discontinuous systems shown in Eq. (18), an approximation of the energy flow from system 2 to 3 can be obtained

$$q_{23} = \frac{1}{r_{22} + r_{33}}\begin{bmatrix}\tau_{23}c_{g2}A_2 & -\tau_{32}c_{g3}A_3\end{bmatrix}\begin{Bmatrix}e_2\\ e_3\end{Bmatrix}. \tag{28}$$

For the continuous system, an estimate of the energy flow at the interelement boundaries can be written as

$$q_{21} = \frac{c_{g2}^2 A_2}{\eta_2\omega}\frac{e_2 - e_1}{\Delta x_{12}}. \tag{29}$$

Substitution of Eqs. (28) and (29) into the energy balance equation for element 2, $q_{21} + q_{23} + \Pi_{\text{diss}} = \Pi_{\text{in }2}$, yields

$$-\frac{c_{g1}^2}{\eta_1\omega L_1\Delta x_{12}}A_1L_1e_1 + \left(\omega\eta_2 + \frac{c_{g2}^2}{\eta_2\omega L_2\Delta x_{12}} + \frac{c_{g2}}{L_2}\frac{\tau_{23}}{r_{22}+r_{33}}\right)A_2L_2e_2 - \frac{c_{g3}}{L_3}\frac{\tau_{32}}{r_{22}+r_{33}}A_3L_3e_3 = \Pi_{\text{in }2}. \tag{30}$$

Note that $A_1 = A_2$ in the three-beam case shown in Fig. 3. The corresponding equations for elements 1 and 3 are

$$\left(\omega\eta_1 + \frac{c_{g1}^2}{\eta_1\omega L_1\Delta x_{12}}\right)A_1L_1e_1 - \frac{c_{g2}^2}{\eta_2\omega L_2\Delta x_{12}}A_2L_2e_2 = \Pi_{\text{in}1} \tag{31}$$

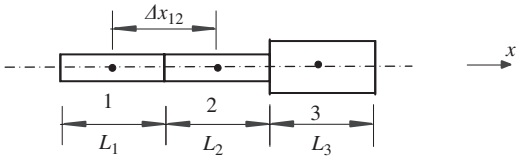

Fig. 3. Coupled three-element beam model with continuous and discontinuous joints.

and

$$-\frac{c_{g2}}{L_2}\frac{\tau_{23}}{r_{22}+r_{33}}A_2L_2e_2+\left(\omega\eta_3+\frac{c_{g3}}{L_3}\frac{\tau_{32}}{r_{22}+r_{33}}\right)A_3L_3e_3=\Pi_{\text{in}3}. \tag{32}$$

The three equations can be assembled into a matrix equation to model the energy flow in the three-element system. In order to write the matrix equation in more concise form and to be able to compare the resulting matrices to SEA matrices, the total energy in the element, $E_i=A_iL_ie_i$, will be used, and two coupling factors will be defined:

$$\eta^c_{eij}=\frac{2c_g^2}{\eta\omega^2L_i(L_i+L_j)}, \tag{33}$$

to model the connection between the continuous systems, and

$$\eta^{dc}_{eij}=\frac{c_{gi}}{\omega L_i}\frac{\tau_{ij}}{r_{ii}+r_{jj}}\approx\frac{c_{gi}}{\omega L_i}\frac{\tau_{ij}}{2-\tau_{ij}-\tau_{ji}}, \tag{34}$$

to model a conservative joint at the discontinuity. The EFEM^0 equations for the three-element system shown in Fig. 3 can be written in matrix form as

$$\begin{bmatrix}(\eta_1+\eta^c_{e12})\omega & -\eta^c_{e21}\omega & 0\\ -\eta^c_{e12}\omega & (\eta_2+\eta^c_{e21}+\eta^{dc}_{e23})\omega & -\eta^{dc}_{e32}\omega\\ 0 & -\eta^{dc}_{e23}\omega & (\eta_3+\eta^{dc}_{e32})\omega\end{bmatrix}\begin{Bmatrix}E_1\\E_2\\E_3\end{Bmatrix}=\begin{Bmatrix}\Pi_{\text{in}1}\\\Pi_{\text{in}2}\\\Pi_{\text{in}3}\end{Bmatrix}. \tag{35}$$

Eq. (35), which has been derived using a finite volume implementation of an EFA equation, has the same structure as the SEA matrix equation, which was derived for lightly damped, weakly coupled modal systems with high modal overlap. Many of the terms are the same, particularly those associated with power input and dissipation of energy within the element. However, two extensions of SEA are derived using the EFEM^0 approach.

Typical SEA coupling loss factors for connected systems (the discontinuous case) are either [13]

$$\eta_{12}=\frac{c_{g1}}{\omega L_1}\frac{\tau_{12}}{2-\tau_{12}}, \tag{36}$$

or

$$\eta_{12}=\frac{c_{g1}}{\omega L_1}\frac{\tau_{12}}{2}. \tag{37}$$

Eq. (34) has been derived for a general problem including strong coupling and significant energy flow from either side of the joint. The denominator of Eq. (34) contains additional terms relative to Eqs. (36) and (37). All three expressions are similar for weak coupling when the transmission coefficients are close to zero but differ when the transmission coefficient is significant. The additional terms in the denominator of Eq. (34) account for the effects of strong coupling and significant energy flow from either side of the joint.

The formulation of the apparent "coupling loss factor" for continuous, damped subsystems in Eq. (33) is novel. No similar factor has been derived for SEA. This formulation allows the division of continuous subsystems into elements. This is particularly helpful for systems with significant damping where the decay of energy within the system must be modeled.

4. EFA and modal solutions for one- and two-dimensional systems

EFA and EFEM^0 solutions will be compared to analytical solutions for simple 1-D and 2-D systems. A hybrid EFA and EFEM^0 method will also be utilized to model the response of damped point-driven plates. The solutions for each of the approaches are derived in this section.

4.1. EFA solution for one-dimensional beams

The general solution of the 1-D EFA governing equation for the far field, space-averaged energy density in a beam can be expressed as

$$e = C_1 \exp(\alpha x) + C_2 \exp(-\alpha x), \tag{38}$$

where $\alpha = \eta\omega/c_g$, and the constants C_1 and C_2 are determined from the boundary conditions. For a clamped beam excited by a harmonic point force as shown in Fig. 4, the energy flow at the right end ($x = 0$) is zero

$$I(x=0) = -\frac{c_g^2}{\eta\omega}\frac{\mathrm{d}e}{\mathrm{d}x}\bigg|_{x=0} = -\frac{c_g^2}{\eta\omega}(\alpha C_1 - \alpha C_2) = 0. \tag{39}$$

Thus, $C_1 = C_2 = C$ (constant), and

$$e = 2C\cosh(\alpha x). \tag{40}$$

The energy flow at the left end ($x = -L$) is

$$I(x=-L) = -\frac{c_g^2}{\eta\omega}\frac{\mathrm{d}e}{\mathrm{d}x}\bigg|_{x=-L} = \frac{\Pi_{\mathrm{in}}}{A}, \tag{41}$$

where Π_{in} is the power input and A is the cross-sectional area. Substitution of the solution (Eq. (38)) into the boundary condition (Eq. (41)) yields

$$C = \frac{\Pi_{\mathrm{in}}}{2\eta\omega A}\frac{\alpha}{\sinh(\alpha L)}. \tag{42}$$

Thus, the EFA solution for the 1-D beam is

$$e_{EFA}(x) = \frac{\Pi_{\mathrm{in}}}{\eta\omega A}\frac{\alpha\cosh(\alpha x)}{\sinh(\alpha L)}. \tag{43}$$

4.2. EFA plane wave solution for rectangular plate

The EFA equation for a point-excited rectangular plate assuming damped plane wave behavior [10] is

$$-\frac{c_g^2}{\eta\omega}\left(\frac{\partial^2 e}{\partial x^2} + \frac{\partial^2 e}{\partial y^2}\right) + \eta\omega e = \Pi_{\mathrm{in}}\delta(x - x_0)\delta(y - y_0). \tag{44}$$

The solution of this equation can be expanded as a sum of the cosine functions

$$e = \sum_{m=0}^{\infty}\sum_{n=0}^{\infty} A_{mn}\cos(m\pi x/a)\cos(n\pi y/b). \tag{45}$$

Substituting Eq. (45) into Eq. (44) yields

$$\sum_{m=0}^{\infty}\sum_{n=0}^{\infty}\left\{(c_g^2/\eta\omega)[(m\pi/a)^2 + (n\pi/b)^2] + \eta\omega\right\}A_{mn}\cos(m\pi x/a)\cos(n\pi y/b) = \Pi_{\mathrm{in}}\delta(x - x_0)\delta(y - y_0). \tag{46}$$

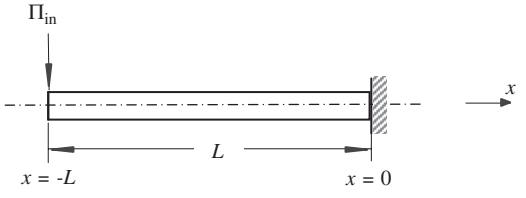

Fig. 4. Free-clamped beam with power input at the free end.

Using Fourier series methods, the EFA energy density solution assuming damped plane waves for a rectangular plate excited at point (x_0, y_0) can be expressed as

$$e = \sum_{m=0}^{\infty}\sum_{n=0}^{\infty} \frac{\Pi_{\text{in}} \cos(m\pi x_0/a)\cos(n\pi y_0/b)}{C_{mn}\{(c_g^2/\eta\omega)[(m\pi/a)^2 + (n\pi/b)^2] + \eta\omega\}} \cos(m\pi x/a)\cos(n\pi y/b), \tag{47}$$

where the coefficient C_{mn} is

$$C_{mn} = \begin{cases} ab/4 & \text{for } m \neq 0 \quad \text{and } n \neq 0, \\ ab/2 & \text{for } m = 0, n \neq 0 \quad \text{or } n = 0,\ m \neq 0, \\ ab & \text{for } m = 0 \quad \text{and } n = 0. \end{cases} \tag{48}$$

4.3. Modal solution for a rectangular plate

The equation of motion for the transverse displacement of an isotropic plate is

$$D\left(\frac{\partial^4 w}{\partial x^4} + 2\frac{\partial^4 w}{\partial x^2\,\partial y^2} + \frac{\partial^4 w}{\partial y^4}\right) + \rho h \frac{\partial^2 w}{\partial t^2} = 0. \tag{49}$$

The bending stiffness D is

$$D = \frac{Eh^3}{12(1-\mu^2)}, \tag{50}$$

where E is Young's modulus, μ is Poisson's ratio, and h is the thickness of the plate.

For a simply supported rectangular plate, the displacements and the moments at the boundaries are zero

$$w(0, y, t) = w(a, y, t) = w(x, 0, t) = w(x, b, t) = 0, \tag{51}$$

$$M_x(0, y, t) = M_x(a, y, t) = 0, \tag{52}$$

$$M_y(x, 0, t) = M_y(x, b, t) = 0. \tag{53}$$

The forced response can be expressed as a modal superposition of the form

$$w(x, y, t) = \sum_{m=1}^{\infty}\sum_{n=1}^{\infty} A_{mn} \sin(m\pi x/a)\sin(n\pi y/b)\exp(\mathrm{j}\omega t), \tag{54}$$

where A_{mn} is an amplitude coefficient determined from the excitation of the problem. For a simply supported plate excited by a point force F_0 at the center, the coefficient A_{mn} is evaluated as

$$A_{mn} = \frac{4F_0}{\rho hab} \frac{\sin(m\pi/2)\sin(n\pi/2)}{(1 + j\eta)\omega_{mn}^2 - \omega^2}, \tag{55}$$

where the natural frequencies for an isotropic plate [14] are

$$\omega_{mn} = \pi^2 (D/\rho h)^{1/2}[(m/a)^2 + (n/b)^2]. \tag{56}$$

The time-averaged energy density for an isotropic plate can be expressed as

$$e = \frac{1}{4} D\left\{\frac{\partial^2 w}{\partial x^2}\frac{\partial^2 w^*}{\partial x^2} + \frac{\partial^2 w}{\partial y^2}\frac{\partial^2 w^*}{\partial y^2} + 2\mu\frac{\partial^2 w}{\partial x^2}\frac{\partial^2 w^*}{\partial y^2} + 2(1-\mu)\frac{\partial^2 w}{\partial x\,\partial y}\frac{\partial^2 w^*}{\partial x\,\partial y}\right\} + \frac{1}{4}\left\{\rho h \frac{\partial w}{\partial t}\frac{\partial w^*}{\partial t}\right\}, \tag{57}$$

where the superscript * designates for the complex conjugate. The modal solution is substituted into Eq. (57) to calculate energy density.

The frequency-averaged energy density was calculated using a sum of the energy density at N frequencies

$$\bar{e} \approx \frac{1}{\Delta f}\sum_{n=1}^{N} e\delta f, \tag{58}$$

where N is

$$N = \frac{f_u - f_l}{\delta f} + 1, \tag{59}$$

where δf is the frequency increment, which could be chosen to be less than one-half the average separation of resonant frequencies $\overline{\delta f}$ [5]. The average frequency spacing between resonances in a 2-D system is [13]

$$\overline{\delta f}^{2D} = \frac{1}{2\pi n(f)} = \frac{c_g^2}{4\pi fab}, \tag{60}$$

where $n(f)$ is the modal density.

4.4. Hybrid method

The EFA plane wave equation was derived using a damped plane wave assumption, and thus, represents well the energy distribution in a damped reverberant field. Where the direct field of a source is dominant, wave propagation is primarily in terms of cylindrical waves for 2-D systems, or spherical waves for 3-D systems. The EFA equation based on superimposed damped plane waves is not a good model of the response of such systems.

A hybrid energy modeling method was developed by Smith [15] to address this problem. The general technique is to separate the contributions of the direct field and the reverberant field and predict responses of these two fields independently. The direct field is calculated assuming the plate is infinitely large. The power entering the reverberant field is assumed to be the power from the direct field reflected at the boundary of the finite system. The overall response is the superposition of the two fields.

For numerical implementation using the EFEM^0 formulation, the problem domain is discretized into finite volumes. The power input to the EFEM^0 is modeled as the intensity at the boundary due to the direct field, which is assumed to be reflected into the reverberant field at the boundary or transmitted into connected systems. The direct field energy density for each volume is calculated from the energy density at the location of the center node of the finite volume relative to the source. The total response for each control volume can be obtained by superposition of the two solutions.

As a simple example of this implementation, a plate shown in Fig. 5 is considered. For S on the boundary surface of a region T in space, $\vec{n}$ is the outer unit normal vector of S. The direct field power flow from a point source to a small surface area ΔA is equal to $\vec{I}\cdot\vec{n}\Delta A$, where $\vec{I}\cdot\vec{n}$ is the normal component of $\vec{I}$ in the direction of $\vec{n}$. For the EFEM^0 numerical implementation, the magnitude of the intensity at a point (j) due to the direct field is

$$I_d^{(j)} = c_g e_d^{(j)} = \frac{\Pi_{\text{in}}}{2\pi h r^{(j)}}\exp(-\eta\omega r^{(j)}/c_g), \tag{61}$$

where $r^{(j)}$ is the distance from the excitation point (x_0, y_0) to the center of the element $(x^{(j)}, y^{(j)})$, and is calculated by

$$r^{(j)} = \sqrt{(x^{(j)} - x_0)^2 + (y^{(j)} - y_0)^2}. \tag{62}$$

$r^{(j)}$ can also be expressed as

$$r^{(j)} = d/\cos\theta, \tag{63}$$

where d is the normal distance from the excitation point to the boundary, and θ is the angle between a radial vector from the source and the normal vector of the boundary as shown in Fig. 5.

The normal component of the direct field intensity in the direction perpendicular to the boundary is $I_d^{(j)}\cos\theta$. Then the resulting power incident on the boundary is $I_d^{(j)}\cos\theta\Delta A^{(j)}$, where $\Delta A^{(j)}$ is the boundary

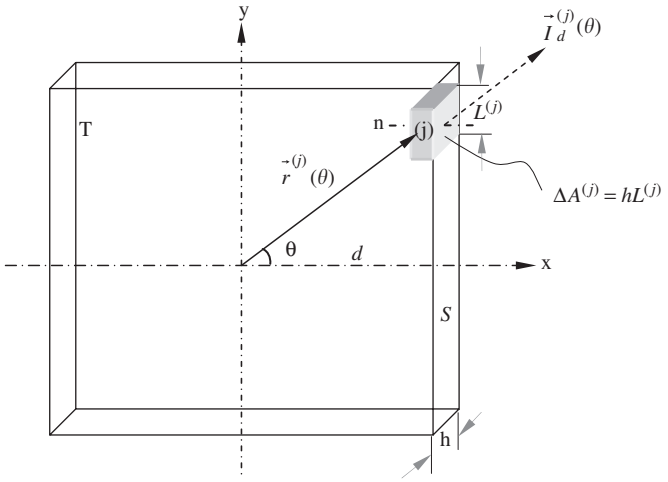

Fig. 5. One element on the plate boundary.

elemental area, $\Delta A^{(j)} = hL^{(j)}$. Assuming $r_{11}(\theta)$ is the reflection coefficient at the location, the power reflected into the element (j) of the reverberant field along the boundary is

$$\Pi_v^{(j)}\big|_\Gamma = r_{11}(\theta) I_d^{(j)} \cos\theta \Delta A^{(j)}. \tag{64}$$

Substitution of Eqs. (61)–(63) into Eq. (64) gives

$$\Pi_v^{(j)}(\theta)\big|_\Gamma = r_{11}(\theta) D(\theta) \beta^{(j)} \Pi_{\text{in}}, \tag{65}$$

where $D(\theta)$ is a directivity function expressed as

$$D(\theta) = \cos^2\theta \exp(-\eta\omega d/c_g \cos\theta) \tag{66}$$

and $\beta^{(j)}$ is defined as

$$\beta^{(j)} = L^{(j)}/2\pi d. \tag{67}$$

The elemental reverberant power is a function of angle θ and can be incorporated into the input power vector of the global matrix of the EFEM^0 model.

5. Applications and results

In this section, the results for SEA, EFEM^0, and hybrid approaches will be compared to analytical predictions for moderately damped beams and plates to illustrate the applicability and limits of each of the methods. In each case the SEA model was developed using a single degree of freedom for each subsystem and the result will be plotted as uniform energy density over the entire subsystem.

5.1. EFEM^0 convergence study

In order to do a convergence study, a single uniform damped beam with simply supported boundary conditions is studied using EFEM^0 theory. The beam is excited using a transverse harmonic force at the center location. The length of the beam is 4 m and the damping loss factor is 0.24. Since EFEM^0 allows the discretization of each subsystem to improve the accuracy of the prediction, the beam is divided into a number of elements. An analytical EFA solution is also obtained for validation. The EFEM^0 predictions of energy density at one point (1 m away from the end) of the beam are shown in Fig. 6. The accuracy of EFEM^0 prediction increases as more elements are used, and converges to the EFA analytical solution, which represents the locally space-averaged value of the responses well.

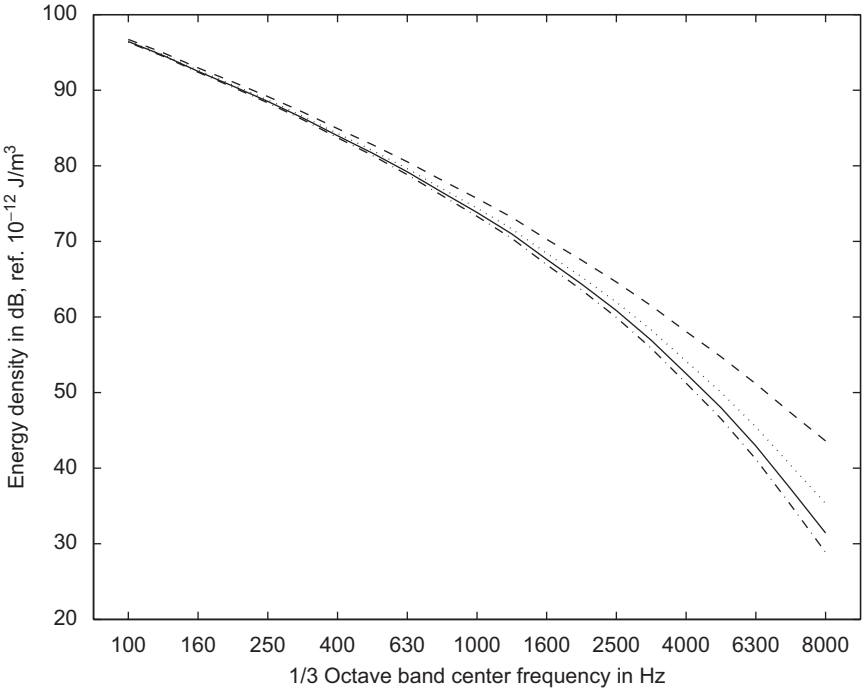

Fig. 6. Predictions of energy density using EFEM^0 coupling loss factors when dividing one uniform damped beam into n subsystems: (- · - · -) EFA analytical solution; (- - - -) EFEM^0, $n = 8$; (…) EFEM^0, $n = 16$; (—) EFEM^0, $n = 32$.

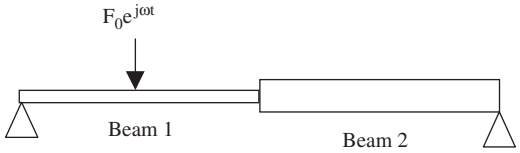

Fig. 7. Two coupled beams with simply supported boundary conditions.

5.2. Coupled beams

The coupled beams shown in Fig. 7 with simply supported boundary conditions were also studied. The physical properties are listed in Table 1. Analytical solutions were obtained using a wave solution for Euler–Bernoulli beam theory. The predictions using the three coupling loss factor relationships (Eqs. (34), (36) and (37)) are compared for three cases: strong coupling ($\tau_{12} = 0.9994$), medium coupling ($\tau_{12} = 0.6289$) and weak coupling ($\tau_{12} = 0.2356$). As shown in Figs. 8–10(a), the predictions using the new η_{eij}^{dc} expressed in Eq. (34) for discontinuous joint match the analytical solutions for all three cases. For weak coupling case predictions as shown in Fig. 10, the difference between the predictions using the three equations is slight. However, for the strong coupling case shown in Fig. 8, the predictions using Eqs. (36) and (37) overestimate the energy density jump at the joint. This investigation shows that the coupling loss factor formulation expressed in Eq. (34) is suitable for both strong and weak coupling cases and is an improvement relative to SEA formulations for strong coupling cases.

5.3. Rectangular plates

The three numerical methods, SEA, EFEM^0 and the hybrid-EFEM^0 method, were compared to the analytical solution for the prediction of energy density for a point-driven plate with the properties listed in Tables 2 and 3. This is a relatively demanding case and is not necessarily typical of applications where

Table 1
Physical parameters of the two beams

	Beam 1	Beam 2		
		Case I	Case II	Case III
Cross-sectional area (m^2)	$A_1 = 4 \times 10^{-4}$	$A_2 = 1.2A_1$	$A_2 = 6A_1$	$A_2 = 16A_1$
Area moment of inertia (m^4)	$I_1 = 1.33 \times 10^{-8}$	$I_2 = 1.44I_1$	$I_2 = 36I_1$	$I_2 = 256I_1$
Young's modulus (Pa)	$E_1 = 7.1 \times 10^{10}$	$E_2 = E_1$	$E_2 = E_1$	$E_2 = E_1$
Density (kg/m^3)	$\rho_1 = 2.7 \times 10^3$	$\rho_2 = \rho_1$	$\rho_2 = \rho_1$	$\rho_2 = \rho_1$
Loss factor	$\eta_1 = 0.25$	$\eta_2 = \eta_1$	$\eta_2 = \eta_1$	$\eta_2 = \eta_1$
Length (m)	$L_1 = 2$	$L_2 = L_1$	$L_2 = L_1$	$L_2 = L_1$

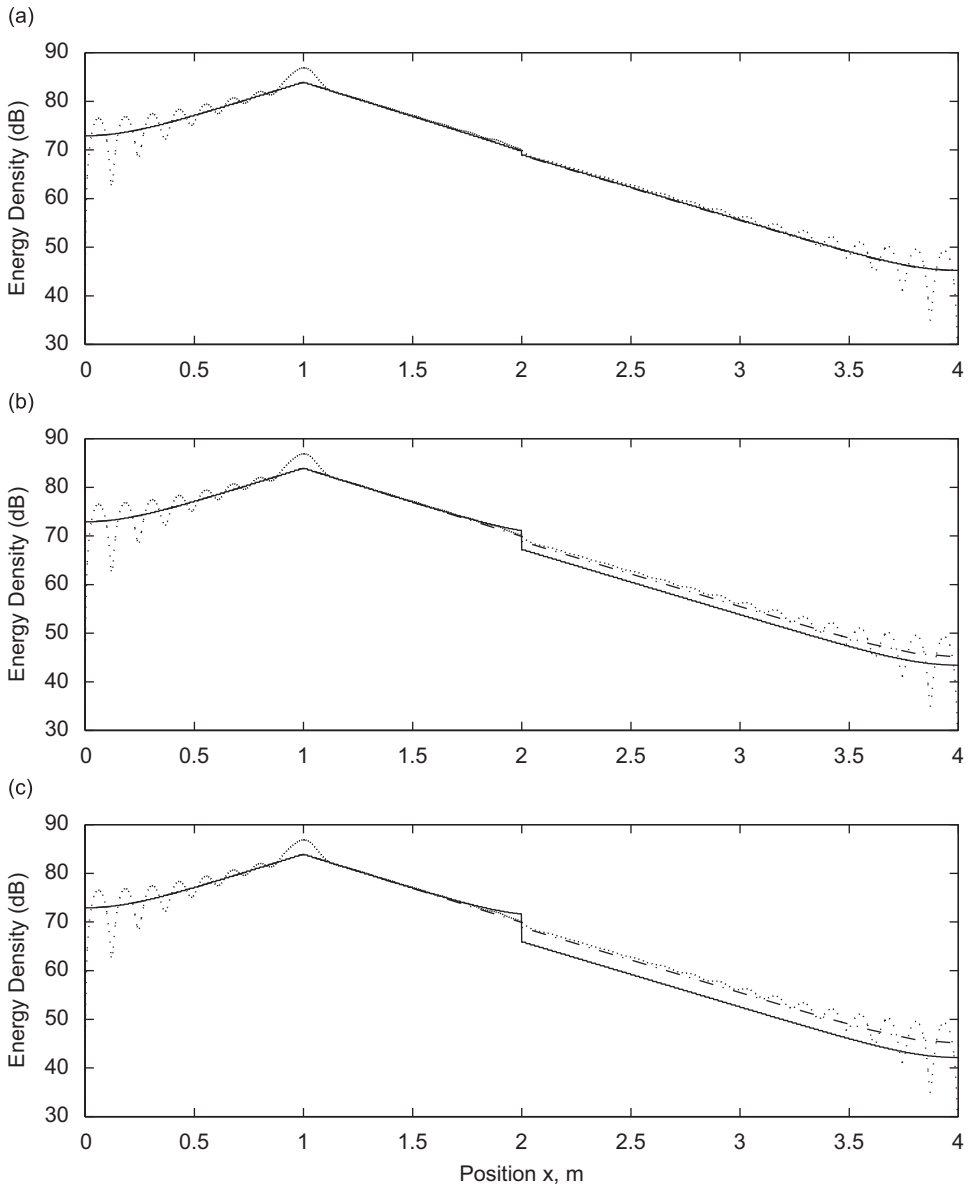

Fig. 8. Comparison of EFEM^0 prediction using different coupling loss factor equations for two strongly coupled beams at 3150 Hz (Case I: $\tau_{12} = 0.9994$): (…) analytical wave solution; (- · · · -) EFA analytical solution; (—) EFEM^0 prediction using: (a) Eq. (34), (b) Eq. (36), and (c) Eq. (37).

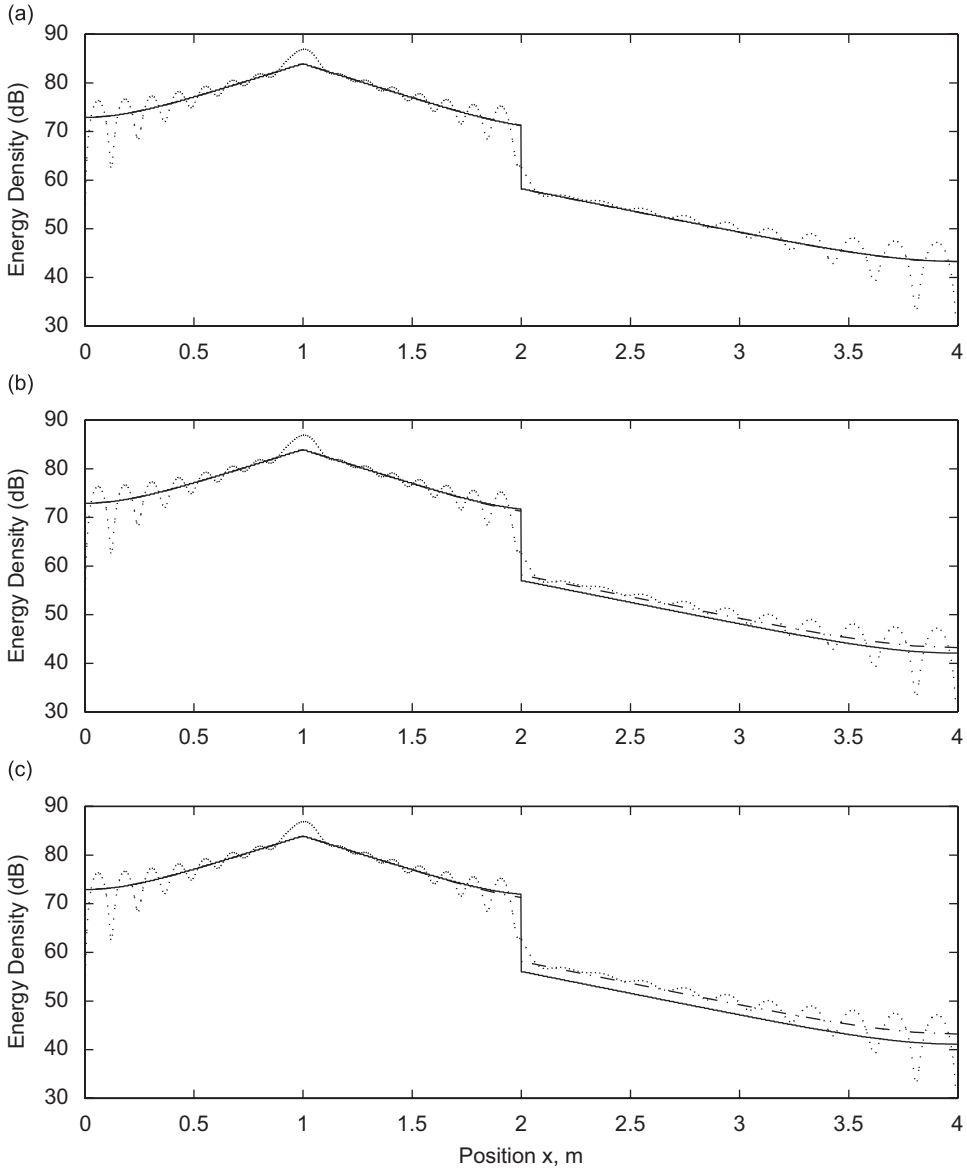

Fig. 9. Comparison of EFEM^0 prediction using different coupling loss factor equations for two coupled beams at 3150 Hz (Case II: $\tau_{12} = 0.6289$): (…) analytical wave solution; (- · - · -) EFA analytical solution; (—) EFEM^0 prediction using: (a) Eq. (34), (b) Eq. (36) and (c) Eq. (37).

subsystems are not directly excited (e.g., act only as conductors of energy) or cases where the source loading is distributed. However, this case is useful to illustrate the differences between the methods, which occur particularly where there is significant damping and localized excitation.

The predictions of the hybrid-EFEM^0 method for plates with simply supported boundaries are shown in Figs. 12–15, compared with the frequency-averaged modal solutions for the plate. The equivalent radius of a rectangular plate was calculated by $R = \sqrt{ab/\pi}$, where a and b are the edge length of the corresponding rectangular plate. The variation of the parameter $\eta\omega R/c_g$ is obtained by adjusting the damping loss factor as shown in Table 3. The results are plotted for the prediction along the x' axis from point O' to P' in Fig. 11, where O' is the center of the plate, P' is the intersection point of the boundaries of the square plate and the equivalent circular plate, and the distance $|O'P'| = R$.

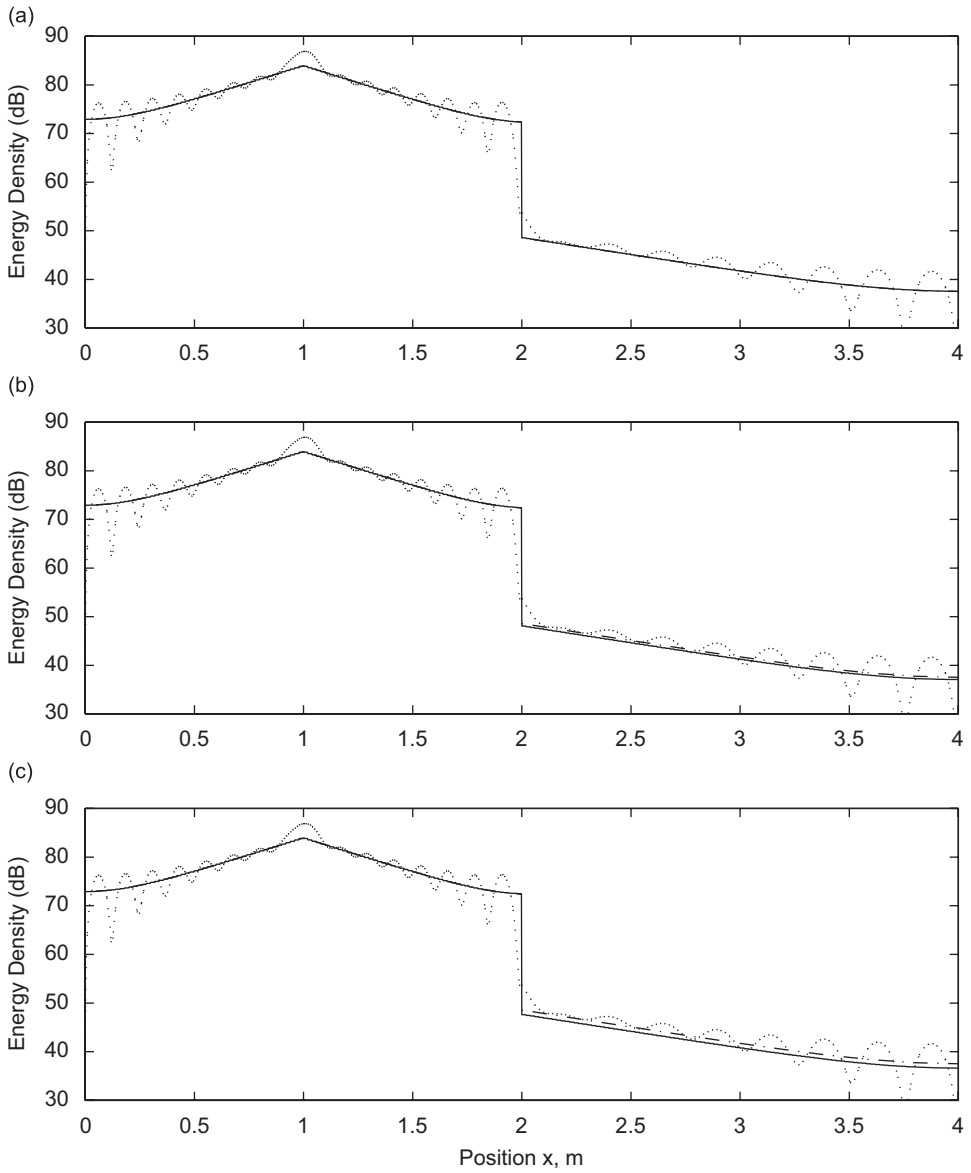

Fig. 10. Comparison of EFEM^0 prediction using different coupling loss factor equations for two weakly coupled beams at 3150 Hz (Case III: $\tau_{12} = 0.2356$): (…) analytical wave solution; (- · - · -) EFA analytical solution; —, EFEM^0 prediction using: (a) Eq. (34), (b) Eq. (36) and (c) Eq. (37).

Table 2
Physical properties of the isotropic square plates

	Properties
Young's modulus (Pa)	2×10^8
Poisson's ratio	0.5
Density (kg/m^3)	1100
Thickness (m)	0.01
Frequency (Hz)	1000
Edge length (m)	1.5
Equivalent radius of circular plate (m)	0.846

Table 3
Loss factor and αR values for case studies

	Loss factor	Parameter $\alpha R = \eta\omega R/c_g$
Case 1	0.001	0.03
Case 2	0.01	0.3
Case 3	0.04	1.1
Case 4	0.25	7.0

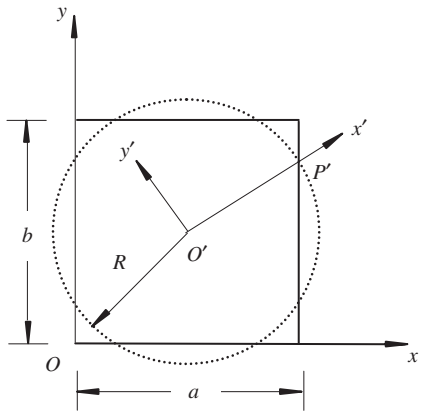

Fig. 11. The square plate and the equivalent circular plate.

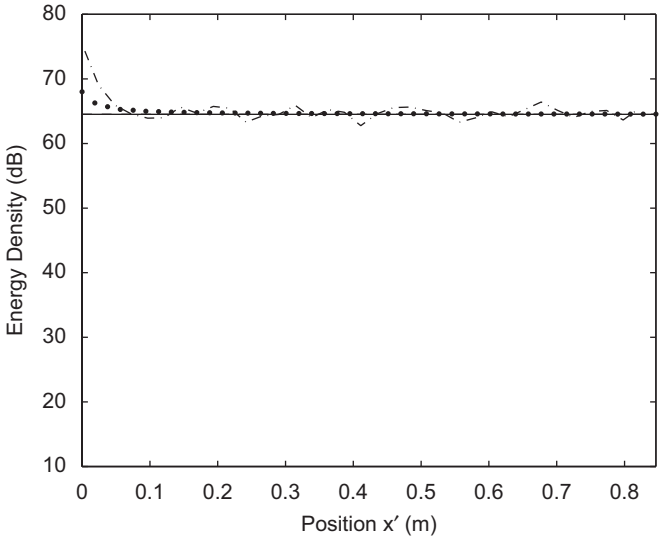

Fig. 12. Energy density predictions for square plate (Case 1: $\alpha R = 0.03$): (- · - · -) modal solution (frequency-averaged); (—) EFA plane wave solution; (- - - -, SEA prediction; (●●●) hybrid-EFEM^0 prediction.

The point source in the plate creates a direct field. For lightly damped cases, the direct field will be dominant in only a small region near the source. For moderately damped systems, the direct field becomes more significant. For heavily damped systems, the direct field dominates the response. All three numerical methods are based on principles of energy conservation. Thus, the total power dissipated will be equal to the power input. Since SEA and EFEM^0 under predict energy flow in the direct field, and thus under predict the energy density in the direct field, the methods over predict the energy density in the reverberant field. The EFEM^0

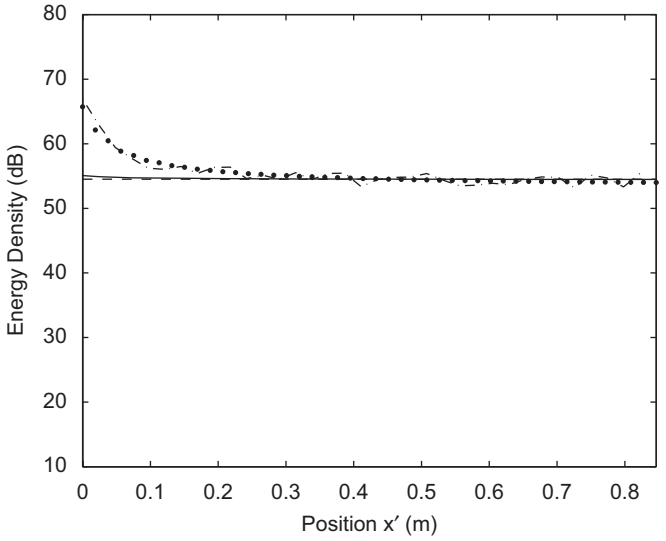

Fig. 13. Energy density predictions for square plate (Case 2: $\alpha R = 0.3$): (- · · ·), modal solution (frequency-averaged); (—) EFA plane wave solution; (- - - -) SEA prediction; and (●●●) hybrid-EFEM^0 prediction.

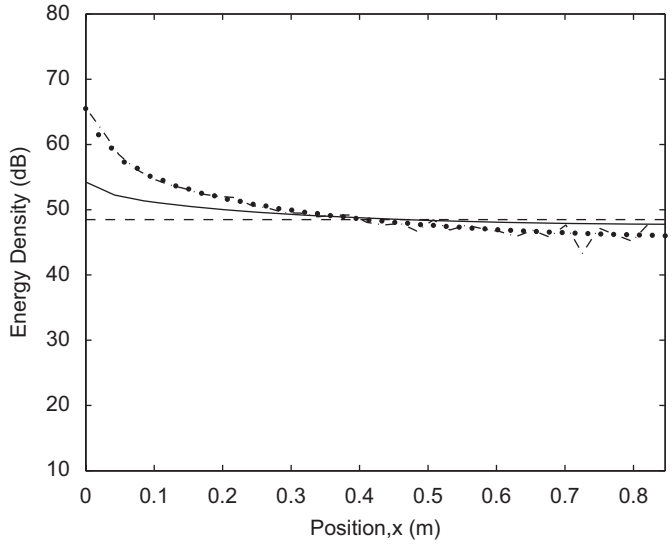

Fig. 14. Energy density predictions for square plate (Case 3: $\alpha R = 1.1$): - · · · -, modal solution (frequency-averaged); (—) EFA plane wave solution; (- - - -) SEA prediction; and (●●●) hybrid-EFEM^0 prediction.

solution by itself is an improvement over SEA but does not appreciably expand the range of applicability of energy-based approaches for the point driven, damped plates. The combination of the EFEM^0 and a direct field solution, as implemented here for the hybrid method, is useful for all cases including direct field dominant cases.

6. Conclusion

The EFEM^0 formulation is developed using wave propagation and averaging techniques and implemented using the finite volume method. The formulation is a new approach and results in less degrees of freedom for a model. The resulting formulation can be implemented with SEA software and extends SEA application to

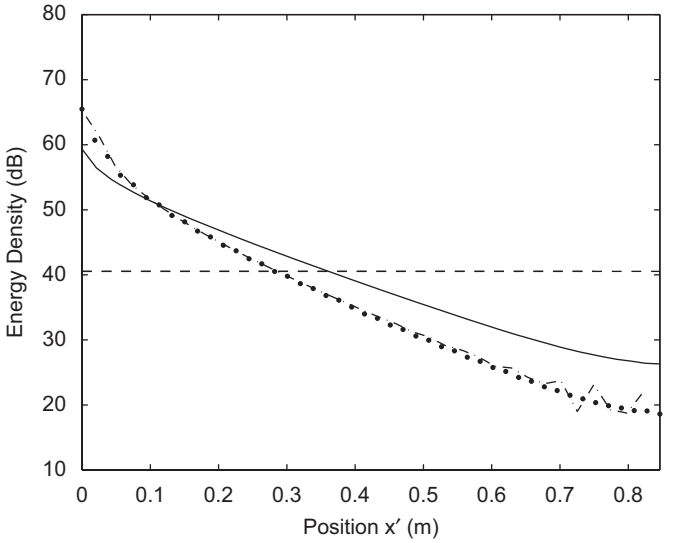

Fig. 15. Energy density predictions for square plate (Case 4: $\alpha R = 7.0$): (- · - · -) modal solution (frequency-averaged); (—) EFA plane wave solution; (- - - -) SEA prediction; and (●●●) hybrid-EFEM^0 prediction.

moderately damped systems with strong coupling. Wang et al. [16] combined the EFEM^0 technique with SEA for sound package optimization of a trimmed van. Wang et al. [17] applied the EFEM^0 in SEA model for exterior acoustic modeling of a truck. Klos [18] also applied the EFEM^0 technique for point-excited shells. For lightly damped systems, both SEA and EFEM^0 methods produce an acceptable model. For moderately damped 2-D systems, the EFEM^0 method produces an acceptable model when augmented using a direct field component. One approach for implementation of the hybrid method using SEA software was illustrated and produced excellent results for point driven plates. For heavily damped systems, the direct field is dominant. While the hybrid EFEM^0 is capable of modeling such problems, a solution using only direct field theory is probably sufficient for most purposes.

References

[1] V.D. Belov, S.A. Rybak, Applicability of the transport equation in the one-dimensional wave-propagation problem, *Journal of Soviet Physics-Acoustics* 21 (2) (1975) 110–114.
[2] V.D. Belov, S.A. Rybak, B.D. Tartakovskii, Propagation of vibrational energy in absorbing structures, *Journal of Soviet Physics-Acoustics* 23 (2) (1977) 115–119.
[3] D.J. Nefske, S.H. Sung, Power flow finite element analysis of dynamic systems: basic theory and application to beams, *Journal of Vibration, Acoustics, Stress, and Reliability in Design* 111 (1989) 94–100.
[4] J.C. Wohlever, R.J. Bernhard, Mechanical energy flow models of rods and beams, *Journal of Sound and Vibration* 153 (1992) 1–19.
[5] P.E. Cho, Energy Flow Analysis of Coupled Structures, Ph.D. Thesis, Purdue University, 1993.
[6] R.H. Lyon, G. Maidanik, Power flow between linearly coupled oscillators, *Journal of the Acoustical Society of America* 34 (1962) 623–639.
[7] J.L. Guyader, C. Boisson, C. Lesueur, Sound transmission by coupled structures: application to flanking transmission in building, *Journal of Sound and Vibration* 106 (1986) 289–310.
[8] S. Wang, High Frequency Energy Flow Analysis Methods: Numerical Implementation, Applications, and Verification, Ph.D. Thesis, Purdue University, 2000.
[9] R.S. Langley, On the vibrational conductivity approach to high frequency dynamics for two-dimensional structural components, *Journal of Sound and Vibration* 182 (1995) 637–657.
[10] O.M. Bouthier, R.J. Bernhard, Simple models of the energetics of transversely vibrating plates, *Journal of Sound and Vibration* 182 (1995) 149–166.
[11] F. Bitsie, The Structural-acoustic Energy Finite Element Method and Energy Boundary Element Method, Ph.D. Thesis, Purdue University, 1996.
[12] H.K. Versteeg, W. Malalasekera, *An Introduction to Computational Fluid Dynamics: The Finite Volume Method*, Wiley, New York, 1995.

[13] R.H. Lyon, R.G. Dejong, *Statistical Energy Analysis*, second ed., Butterworth-Heinemann, Boston, 1995.
[14] W. Soedel, *Vibrations of Shells and Plates*, Marcel Dekker, New York, 1993.
[15] M.J. Smith, A hybrid energy method for predicting high frequency vibrational response of point-loaded plates, *Journal of Sound and Vibration* 202 (1997) 375–394.
[16] S. Wang, H. Xu, G. Ebbitt, Sound package optimization using an EFEM0-SEA model for a trimmed van, *Proceedings of SAE 01 Noise & Vibration Conference*, Traverse City, MI, 2001.
[17] S. Wang, G. Ebbitt, R.E. Powell, Development of a generic truck SEA model with EFEA–SEA hybrid exterior, *Proceedings of Inter-Noise 02*, Dearborn, MI, 2002.
[18] J. Klos, Modeling Cylindrical Shell Dynamics using Energy Flow Methods: An Analytical and Experimental Validation, M.S. Thesis, Purdue University, 2001.